*Materials Research*. 2022; 25:e20210233
DOI: https://doi.org/10.1590/1980-5373-MR-2021-0233

# Evaluation of the Physical and Biological Properties of Ti-34Nb-6Sn/Mg Alloy Obtained by Powder Metallurgy for Use as Biomaterial

*Mariana Correa Rossi[a,b]*, Fernanda de Castro Stievani[a], João Pedro Hübbe Pfeifer[a], Luis Gallego Martinez[c], Vicente Amigó Borrás[b], Margarida Juri Saeki[d], Ana Liz Garcia Alves[a]*

[a]*Universidade Estadual Paulista Júlio de Mesquita Filho, Departamento de Cirurgia Veterinária e Reprodução Animal, Laboratório de Medicina Regenerativa, Botucatu, SP, Brasil.*
[b]*Universitat Politècnica de València, Institut de Tecnologia de Materials, València, Espanha.*
[c]*Universidade de São Paulo, Instituto de Pesquisas Energéticas e Nucleares, Centro de Ciência dos Materiais e Tecnologia, São Paulo, SP, Brasil.*
[d]*Universidade Estadual Paulista Júlio de Mesquita Filho, Instituto de Biociências de Botucatu, Departamento de Química e Bioquímica, Botucatu, SP, Brasil.*

Received: May 18, 2021; Revised: December 15, 2021; Accepted: January 13, 2022

Ti-34Nb-6Sn alloy were prepare by powder metallurgy milled in two different times (40 and 60 min) using Ti and Nb hydrides with or without Mg, as spacer then sintered at 700ºC and 800ºC. Characterizations were made by scanning electron microscope (SEM), X-ray diffractometer (XRD) and by Archimedes. Microhardness was measured by Vickers microhardness. Mesenchymal stem cells derived from equine bone marrow (BMMSCs) were used to evaluate the sample cytotoxicity. Hydration and dehydration process was confirmed, also the formation of brittle particles during the milling. Materials were structured under α and β phase, and the samples that received Mg as a spacer had slightly lower β phase content compared to samples without Mg, suggesting difficult α→β transformation due to the presence of barriers formed by pores. Mg provided greater porosity, and prepared milled in a shorter time promoted an increase in the macropores. Microhardness was similar to that of commercial materials (i.e., CP-Ti and also to other alloys with similar nominal composition. Cells treated with conditioned medium with the samples showed viability comparable to the control group, and after 48 h of culture on the samples, there was significant growth and more circular morphology, when adhered on materials that received Mg.

**Keywords:** *β titanium alloy, High energy milling, Biocompatibility, Biomedical implant.*

## 1. Introduction

The number of patients requiring orthopedic prostheses has significantly increased, due to the increasing world population and the life expectancy[1,2]. In orthopedic repairing, the most used devices are metallic, ceramic and polymer[3], as they are able to almost recover the function of bone tissue for a long period of time[4]. Among the metallic devices, the most used are stainless steel, Co-Cr alloy, titanium and its alloys such as Ti-6Al-4V[5]. It is known that titanium has adequate characteristics as medical device such as mechanical strength, elastic modulus, low susceptibility to corrosion and good biocompatibility[6-8]. For this reason, the main metallic alloys have titanium in their composition[9,10]. Notwithstanding, the most widely used titanium alloy (Ti-6Al-4V) has aluminum and vanadium, components that are known as cytotoxic and can lead to neurological and respiratory disorders[11,12]. Even so the elastic modulus is as high as 110 GPa while that of the bone is between 10 and 30 GPa.

As they are nontoxic, niobium (Nb) and tin (Sn) are good candidates for synthesis Ti alloys, under suitable conditions, combining good stiffness and increasing the osteointegration[13,14]. Regarding the manufacture of metallic alloys, the powder metallurgy technique is a fast, simple technique and requires temperatures lower than of the melting of component metals and also by the use of hydride. Besides that, can promote milling to the desired particle size with excellent homogeneity it reconciles metals with different melting points[15] and in sintering, hydrogen is eliminated, which contributes to providing a reducing atmosphere.

Introduction of hydrogen atoms in metals are made by interstitial solid solution, where the free sites in the lattice are occupied. Titanium and hydrogen form a simple eutectoid with the α + hydride phases forming directly from the β phase. The strong β stabilizing effect of hydrogen results in a decrease of the α→β transformation temperature from 882°C to a eutectoid temperature of 300°C[16]. The terminal hydrogen solubility in the β phase is about 50 at% at above 600°C while in the α phase, the maximum terminal hydrogen solubility is only about 7 at% at 300°C and decreases rapidly with decreasing temperature. In titanium alloys, like in other group IV transition metals, hydrogen tends to occupy tetrahedral interstitial sites. Due to the relatively open bcc structure of the β phase, hydrogen has a much higher solubility

*e-mail: mariana.rossi@unesp.br

as well as much higher diffusivity in β alloys compared to α alloys. This is also facilitated by the presence of more sites per Ti atom in the β alloys compared to Ti atom in the hcp α alloys (seen Figure 1).

Ti with hcp crystalline structure promotes the metal embrittlement, and then the materials is reduced to fine powders. After, the hydrogen is then removed by heating the material under a vacuum. In more details the main advantages in the use of titanium hydrides are:

I. $TiH_2$ as raw material is cheaper because it is an intermediate product in the HDH-Ti powder production;

II. It achieves higher densification compared to Ti sintered under the same conditions;

III. The brittle behavior of $TiH_2$ helps to fragment particles during pressing improving or increasing the compressibility of the powders;

IV. The lattice defects generated by decomposition reactions of Ti activate the diffusion process, which leads to pore healing and accelerates the chemical homogenization of the final product;

V. Hydrogen released during the transformation to Ti, through the reaction $TiH_2 \rightarrow Ti + H_2$, provides a protective atmosphere for Ti surface that reduces or can also controls the contaminations amount;

Some authors proposed that dehydrogenation occurs with the following sequence: $\delta(TiH_2)$ *Stage I* $\rightarrow \delta(TiH_x)$ *Stage II* $\rightarrow \beta(TiH)_H$ *Stage III* $\rightarrow \beta(TiH)_H + \alpha(TiH)_H$ *Stage IV* $\rightarrow + \alpha(Ti)$[17,18].

In first stage, hydrogen atoms are released and change their position randomly from tetrahedral to octahedral interstitials sites, but keeping the initial face-centered cubic (fcc) structure $\delta(TiH_2)$.

In the second stage, as hydrogen is lost δ-phase is gradually transformed to β-Ti phase that is hydrogen-rich (β-Ti) with a body centered cubic (bcc) crystal structure. Then, the hydrogen is continuously released from β-TiH, and α-TiH (with a hexagonal compact crystal structure) begins to form when the hydrogen amount is low enough (third stage). During 2 and 3 stages, the highest conversation of Ti hydride takes place, achieving up to 80% of dehydrogenation.

The phase transformation model is like a core-shell structure, where ($TiH_x$) constitutes the nucleus, the intermediate layer corresponds to β-TiH and external layer is α-TiH. Finally, complete α-Ti transformation occurs, which means that complete hydrogen elimination is produced in the last stage, which depend on the surface features.

The last theoretical dehydrogenation stage (fourth stage) when the transformation β-H + αH to α-Ti phase takes place, was not expected to happen for the alloyed samples due to the presence of a high quantity of β-stabilizer elements incorporated, which considerably reduced the β *transus* temperature with respect to unalloyed Ti.

As described above, this method can reduce production time and cost, but also the hydrogen can be removed during the dehydrogenation process and the existence of hydrogen atoms can make sintering process carry out easily and provide a contraction even in low temperatures. This preparation process can reduce the oxidation of samples, because of the existence of hydrogen. Allied to powder metallurgy, it is possible to combine spacers particles, which present low boiling point to provide porosity to the materials. Mg has been used for this purpose for the Ti biomaterial production[19,20]. Its solubility is insignificant in Ti, besides, it is very difficult to extend the solubility of Ti in Mg by rapid solidification, such as in powder metallurgy and liquid or solid-state techniques[21]. Liquid state methods are widely used to produce AL, Zn and Mg-based porous materials, due to feasibility to pressing thanks to their low reactivity and low melting points. However, these kinds of techniques are very difficult to be apply due to the high melting point and their excessive chemical affinity to atmospheric gases that rapidly dissolve above 400ºC. Then, solid state or PM as cited can produce porous Ti alloys at much lower temperature and under less chemical reactivity constraints, allowing more precise control of process, variables and pore size.

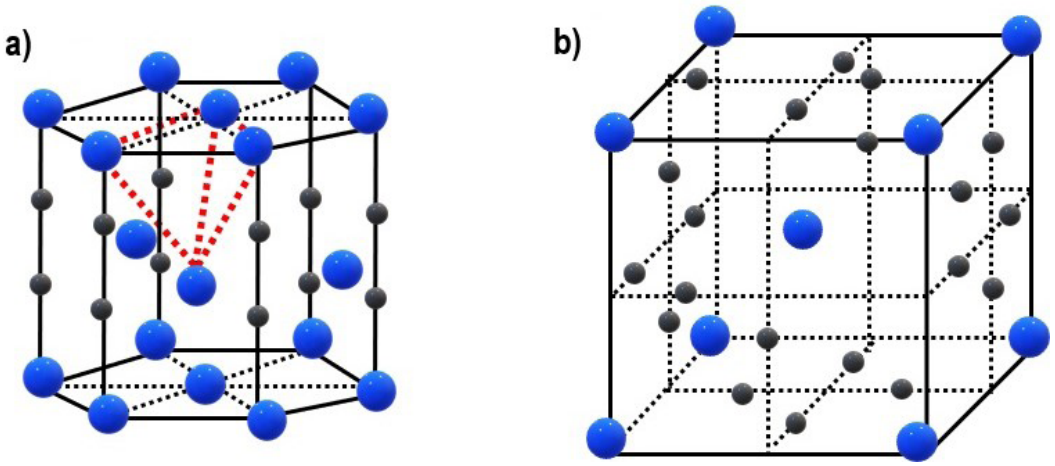


**Figure 1.** Representation of tetrahedral interstitial sites within unit cells a) hcp and b) bcc by the rigid sphere model. Blue spheres refer to titanium atoms and black spheres refer to hydrogen atoms.

Mg has higher solubility in the β-Ti phase, which is stable at high temperatures, according to the Mg-Ti phase diagram[22]. Stable energy conditions are generated above the α-phase transformation temperature. Is that why in this work we used low temperature conditions to create porous Ti alloy.

Also, increases osteoconductive without biomedical inconveniences[23], no separate removal step is required for Mg powders to form pores through their evaporation during the sintering process. Also, Mg vapor can provide a reducing atmosphere to prevent oxidation of titanium[24] among with the dehydrogenation process. As pure Ti has a melting point that greatly exceeds the boiling point of Mg and therefore, alloying of Mg and Ti by conventional methods is extremely difficult[25].

## 2. Main Characteristics of High Energy Milling and Sintering of Ti Alloys with Nb and Sn Alloy Elements

High-energy ball milling (HEBM) is a mechanical deformation process that is frequently used for producing nanocrystalline metals or alloys in powder form. This technique belongs to the comminution or attrition approach.

In the HEBM process, coarse-grained structures undergo disassociation as the result of severe cyclic deformation induced by milling with stiff balls in a high-energy shaker mill. This process has been successfully used to produce metals with minimum particle sizes from 4 to 26 nm. The HEBM is simple and has high potential to scale up to produce huge quantities of materials. However, a serious problem of this technique is the contamination from milling media (balls and vial) and or atmosphere.

Therefore, a number of improvements, including the usages of surfactants, alloy-coated milling media, and protective atmosphere, have been developed to alleviate the contamination problem.

The fine powder (in nano or submicron sizes) produced from ball milling can be consolidated to bulk form for large-scale applications such as hip implants and bone screws.

The synthesis of materials by this technique was first developed in 1970 by John Benjamin[26]

Details about the stages of HEBM was described by Rajeshkanna and Nirmalkumar[27,28].

At the first stage, the powder particles are flattened by the compressive force caused by the impart of the balls. Microforging leads to changes in the shapes of individual particles, or clusters being repeatedly impacted by the balls with high net change in mass.

Later, a significant change occurs as compared to the first one. Cold welding becomes significant and the intimate mixture of the powder constitutints decreases the diffusion distance to the micrometer range. Fracturing and cold welding are the dominant milling process at this stage. Although some dissolution may take place, the chemical composition is still not homogenous. Increase in homogeneity can be achieved during the sintering process.

In order to better understand the consolidation of alloys with high content of β-stabilizer elements of the Ti-Nb-Sn system, a brief description of the binary systems Ti-Nb, Ti-Sn and Nb-Sn will be presented based on their diagrams of phase.

The first thermodynamic studies about Ti-Nb, Ti-Sn and Nb-Sn binary systems were made by Murray, Moiseev, Antipov and Moiseev and Liu[28-31].

The binary phase diagram includes liquid, β-Ti (bcc), α-Ti (hcp) and β-Sn (bct), $Ti_3Sn$, $Ti_2Sn$, $Ti_5Sn_3$ and $Ti_6Sn_5$.

The composition range of solution phase β-Ti and α-Ti in Ti-Sn system is 0-7.5 at% Sn and 0-17% at% Sn. The thermodynamic modeling of Nb-Sn phase diagram was assessed by Toffolon. There exist three solution phases liquid, β-Nb and β-Sn as well three intermediate compounds ($Nb_3SN$, $Nb_6Sn_5$ and $NbSn_2$)[32].

The Ti-Nb phase diagram was proposed by Zhang et al.[33], which contains three stable phases liquid, β(Ti,Nb) and α-Ti. In the work of Wang et al.[34], was studied the equilibrium phases and compositions of Ti-Nb-Sn at 700 ºC. They found that in the Ti-Sn, Nb-Sn and Ti-Nb binary systems description, phases liquid, β(Ti,Nb), α-Ti, $Ti_3Sn$, $Ti_2Sn$, $Ti_5Sn_3$, β-$Ti_6Sn_5$, $Ti_2Sn_3$, $Nb_3Sn$, and $NbSn_2$ should be stable in the Ti-Nb-Sn system at 700 ºC.

They concluded the homogeneity range of phase α-Ti is 0-10.6 at% Sn in Ti-Sn system and 0-2.5 at% Nb in Ti-Nb system, and that of phase β(Ti,Nb) is 14.8-100 at% Nb in Ti-Nb system and 0-2.6 at% Sn in Nb-Sn system.

Phase α-Ti does not exist in Nb-Sn system, and no β phase appears in Ti-Sn system.

The compositions of equilibrium phase β(Ti,Nb) in alloy with specific composition (60.2 at% Ti, 30.6 at% Nb and 9.2 at% Sn) can fit β(Ti,Nb) homogeneity range, and the solubility of Sn in β(Ti,Nb) phase found to extend up to 9.2 at% and the results show that a relative large region of the β(Ti,Nb) continuous bcc solid microstructure at the annealing temperature.

In our previous work we found good mechanical properties with elastic modulus in the range of 18-49 GPa of Ti-34Nb-6Sn/Mg[35,36]. In this way, the Ti-34Nb-6Sn/Mg alloy using titanium and niobium hydrides was synthesized by powder metallurgy technique. Two milling times and two sintering cycles were compared with characteristics of the material obtained for orthopedic purposes.

## 3. Experimental Procedure

### *3.1. Synthesis*

Grade 2 TiH powders (ASTM F67), NbH (99.99%) and atomized Sn (99.50%) were supplied by CBMM (Araxá-MG-Brazil) and Metalpó (São Paulo-Brazil). Quantities to obtain an alloy with mass ratio of 60% in Ti, 34% in Nb and 6% in Sn, and in the case of alloys with Mg it was added in a sufficient quantity to give 2% in relation to the total mass, were mixed in a high energy planetary mill (FRITZCH-model Pulverisette 5) in steel jars, volume= 450 mL, using steel spheres with 5 mm of radius (each balls presented a mass of 4.07g). The ball to powder weight ratio was 10:1. The milling batch had a mass of 40 g for each run, then were used n=98 balls) at 200 rpm in the presence of ethanol, which was placed in sufficient quantity to cover the powders. After for 40 min and 60 min of milling the mixtures were dried under vacuum and compacted uniaxially in a 1 $cm^2$ matrix with cavity cross-section circular at a pressure of 100MPa. The sintering was carried out in two stages: 1) at 400 ºC for

1 h to allow debinding of ethanol and then 700 ºC for 2 h for sintering. This process was realized in samples milled for 40 min. 2) at 400 ºC for 1 h to allow debinding of ethanol and then 800 ºC for 2 h for sintering. This process was realized in samples milled for 60 min. The heat process was made in a high vacuum resistive furnace (COMBUSTOL - model Tubular Oven) coupled to a mechanical pump (Edwards) and diffuser (Edwards), which provided a pressure less than $10^{-2}$ Pa. Before sintering, the furnace chamber was replaced with argon and evacuated twice. The stages of sintering are demonstrated in Figure 2.

### *3.2. Microstructural Characterization*

Metallographic preparation was carried out on all samples, in order to eliminate irregularities and surface oxides. For the metallographic preparation was used standard sandpaper of 220, 320, 400, 600 and 1200 mesh in the presence of water, to avoid overheating. After this stage, they were polished with 0.3µm and 0.05µm alumina (Alcrisa-Teclago). The structural characterization (identification of the present phases) of the powder mixture after milling and sintering of the specimens were made using X-ray diffractometer with Cu Kα radiation (Rigaku-Ultima IV) operating with 0.05 steps at the angles where the diffraction peaks were wider and 0.02 degrees for narrower peaks. Counting times per step were in the order of 10 s. The refinement of the crystalline structure and the quantitative analysis of phases were performed using the Rietveld method, using GSAS software[37]. Semi-quantitative chemical composition and morphological analyzes were performed using a Scanning Electron Microscope (SEM, from FEI, Quanta 200), equipped with a Secondary Electron detector (Everhart-Thornley), Backscattered Electrons and X-ray Dispersive Energy (EDS from Oxford, 51 -XMX1119). The peaks of aluminum (Al), oxygen (O), gold (Au), silicon (Si) and carbon (C) were disregarded, since the presence of these species is due to metallization (Au), sandpaper, sample bonding in the Al stub with C tape and air O.

### *3.3. Hardness test*

The microhardness values of the samples were measured by Vickers microhardness. For optimum accuracy of the measurements, the tests were performed on disks with polished surfaces. The load applied was 300 gf and an indentation time of 60s[38] in a Shimadzu equipment, model HMV-G. The number of indentations in each sample was 5.

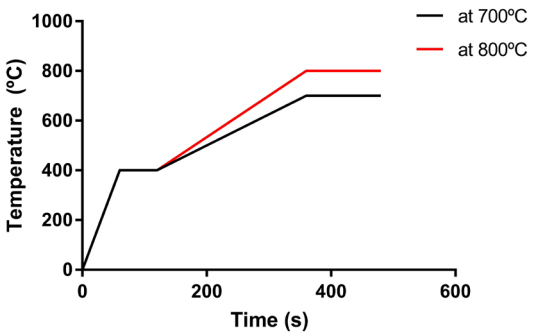


**Figure 2.** Sintering process of Ti-34Nb-6Sn alloy.

### *3.4. Relative Porosity in the sintered materials*

The porosity was determined using the Archimedes principle (relative porosity), following the B328 ASTM standards. Porosity was also assessed by analyzing the images obtained with scanning electron microscopy (SEM) using the software Image J®.

### *3.5. Cell culture and biocompatibility*

First, the disks were cleaned and sterilized in order to avoid possible contamination. Thus, after polishing, each sample was ultrasonically cleaned with acetone, isopropyl alcohol and ultrapure water (18.2 MΩcm) for 15 min. Then, the samples were dried and autoclaved at 120 ºC for 1h. Sterilization was performed for 1 h in order to ensure possible contamination. In addition, there is no evidence of mechanical changes in Ti alloys, after 5 sterilization cycles using the same time and temperature as the present work[39]. In biological assays, mesenchymal stem cells derived from equine bone marrow (BMMSCs) were used. Several studies have been carried out to understand the biological effect of Ti alloys when in contact with bone marrow-derived mesenchymal stem cells[40,41]. These cells are known to have osteogenic differentiation capacity depending on the topography of the surface on which they are in contact[42-44]. In addition, stem cells are the first cells to come into contact with the surface of the implants when implanted, which are then differentiated into bone cells, the so-called osteoblasts. They present a crucial role on to maintaining osseous tissue integrity[45]. Thus, the effect of the materials on the viability of the mesenchymal stem cells derived from equine bone marrow (BMMSCs) were studied by cultivating them in a medium that was conditioned for 24 h with the materials, as established by the ISO 10993-5 standard and described below. The BMMSCs were initially cultured at a ratio of $1x10^5$ cells/well in KnockOut DMEM (ThermoFisher Scientific) culture medium in 96-well plates. These plates were incubated at 37 ºC in the air containing 5% $CO_2$ and kept under these conditions for 24 h. At the same time, only the culture medium was kept incubated in the same conditions with the samples obtained by sintering at 700 and 800ºC. After that time, the cells of the first plate were treated with these conditioned media (Treated), and the control group received only conventional culture medium (Control) in a volume of 100 µL per well. The cell plates were kept at 37ºC for another 24h. Then, the media were aspirated, 100 µl of Diphenyl tetrazolium dimethylthiazole bromide (MTT) (Sigma-Aldrich) (5mg/ml of medium) was added to each well and incubated in the same conditions as above for 3h. Afterwards, the remaining MTT was removed and the formazan crystals formed by the reaction of the MTT salt with the mitochondria of viable cells were dissolved by the addition of 100µl of isopropyl alcohol (Sigma-Aldrich) to each well. Finally, the absorbance of formazan was determined by the colorimetric method in a microplate reader at 570 nm. This experiment was carried out in triplicate. In another assay, the cells morphology and they adhesion on the samples were studied using the same cell line, at a density of $1x10^4$ cells/

well in 24-well plates where the cells were cultured in direct contact with the surface of each sample. The plate was incubated with the respective materials and cells under the same conditions as the experiment above. After 48h, the medium was replaced with a new one, remaining so until completing 48h of culture, when the cells were fixed with glutaraldehyde (2.5%), buffered with PBS (phosphate buffer solution) at 0.2 mol/L. Then they were dehydrated in aqueous solutions with increasing ethanol concentration [7.5% (2x10min), 15% (2x10min), 30% (2x10min), 50% (2x10min), 70% (3x15min), 90% (2x15min) and 100% (2x10min)] and subjected to drying above the critical point in $CO_2$. The specimens were analyzed by SEM after metallization with a gold layer. The use of BMMSCs is approved by the ethics committee and is registered under protocol CEUA 0235/2018.

### *3.6. Statistical analysis*

The experimental results of cell viability, semi-quantitative compositional analysis by EDS and Hardness are presented as a mean ± the measurement deviation value, which was based on the SD here, using error bars in the figures. Each set passed the normality test and a comparison was made between the groups using t-test and Mann-Whitney. The software used was GraphPad Prism v.7.0 and the differences were considered statistically significant when $P < 0.05$.

## 4. Results and Discussion

### *4.1. Characterization of the milled powders obtained by high energy milling*

Figure 3 shows the morphological evolution of the starting powders after milling at 200 rpm at 0, 40 and 60 min, respectively. During the powder milling process, the particles are subject to several mechanical processes, such as plastic deformations and fractures of the elemental powders[46]. In order to promote a decrease in cold welding and reduce its aggregation[47], ethyl alcohol was used. The particles of powder flatten by the constant collisions between the balls of the mill and then lamellar particles are produced. In the first stage, where the particles were just mixed (T0), the particles present irregular and spherical morphologies, depending on the nature of the powders (Figure 3a and a'). By the additional milling, the plastic deformation of the powders leads to fracture work, reducing their sizes, starting the process of microstructure refinement. This occurs at 40 min of milling (Figure 3b and b'). In this stage, the particles do not have spherical morphology, however, the sizes reduction is noticeable, confirming the efficiency of the process. In addition, these characteristics indicate that they have been subject to the physical actions already mentioned. Figure 3c and c' refer to the milling for 60 min, and it is noted that this time was sufficient for the particles to undergo the shear process[48,49] significantly reducing their

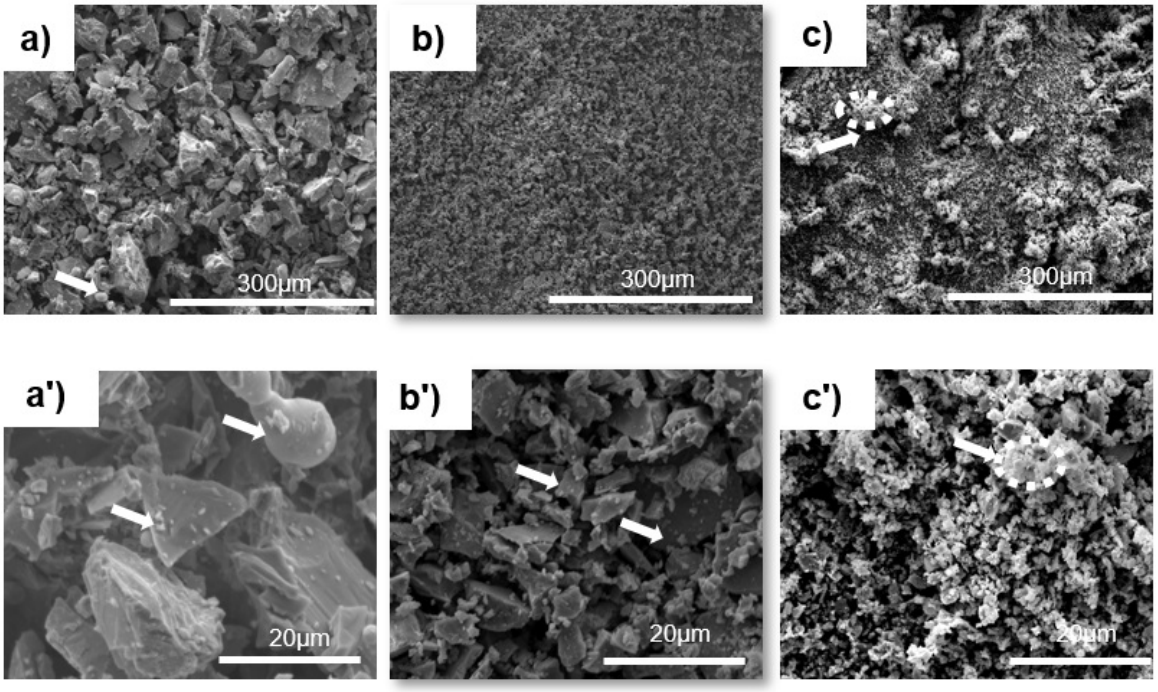


**Figure 3.** Particle size morphology of Ti-H, Nb-H and Sn powders whose mixtures were prepared by milling at 200 rpm for 40 and 60 min obtained by scanning electron microscopy: a) and a') represent the mixture of the powders in time 0 min. The arrows indicate the irregular morphology of the particles; b) and b') represent the powders after grinding for 40 min (magnification of 500 and 2000x). The arrows indicate the decreasing size of particles; and c) and c') represent the powders after grinding for 60 min. The dashed circle indicates clusters of particles more refined.

size. This decrease in size makes the particles more reactive, because the effective contact area increases considerably by several times. According to the literature, smaller and finer particles can fill the spaces between the powders, increasing their packaging[50] and consequently making materials more resistant to fracture. Besides that, a bimodal distribution of large and fine particles is always better for higher packing. However, porosity tends to decrease with that. Such hardening is caused by the interaction of particles with the balls and continuous mechanical impacts[51]. In 60 min, the powders have a greater contact surface and there is an increase in the interaction between them. Particles that are flatter and have a greater contact surface (Figure 3c and c') tend to deform more during compaction process[52]. Thus, a prolonged milling process may not be necessary[53] further presenting a greater tendency to form agglomerates, making the process less effective, in any case, the effect of milling can also be in the case of a mixture of hydrides could not be effective due to fragility. Increasing milling time, the capacity of particles to accept further plastic deformation decreases. As welding is the dominant mechanism in the process, particles morphology changes to flattened particle agglomeration. The last stage involves the fracture of particles, resulting in greater deformation and/or fragmentation[54]. Then their size decreases significantly, causing an increase in agglomerated particles also the resistance to fracture. The increase of fracture resistance and greater cohesion between the particles, with decreasing particle size, cause agglomeration[55]. Self-combustion of the powder was observed with milling time greater than 60 min and/or higher rotation speeds. Thus, to prepare the material with the sintering temperature of 700 ºC, the mixing time of 60 min was used and 40 min for 800 ºC, both at 200 rpm. This combination was used in order to assess whether the refinement of the particles could influence the formation of porosity. The samples powders were also evaluated for the distribution of the elements Ti, Nb, Sn and Mg (Figure 4a and b) using EDS detector. In 40 min it is observed that the elements Ti, Nb and Mg are distributed with relative homogeneity (Figures 4a). Sn particles is more aggregated (Figure 4a), probably because the hardening and fracture phase is late compared to that of other elements. Besides, Sn is more soluble than Nb in Ti[56], thus, its particles can be incorporated easier than Nb, even if agglomerated. In 60 min of milling (Figure 4b), Ti, Nb, Sn and Mg particles are better distributed.

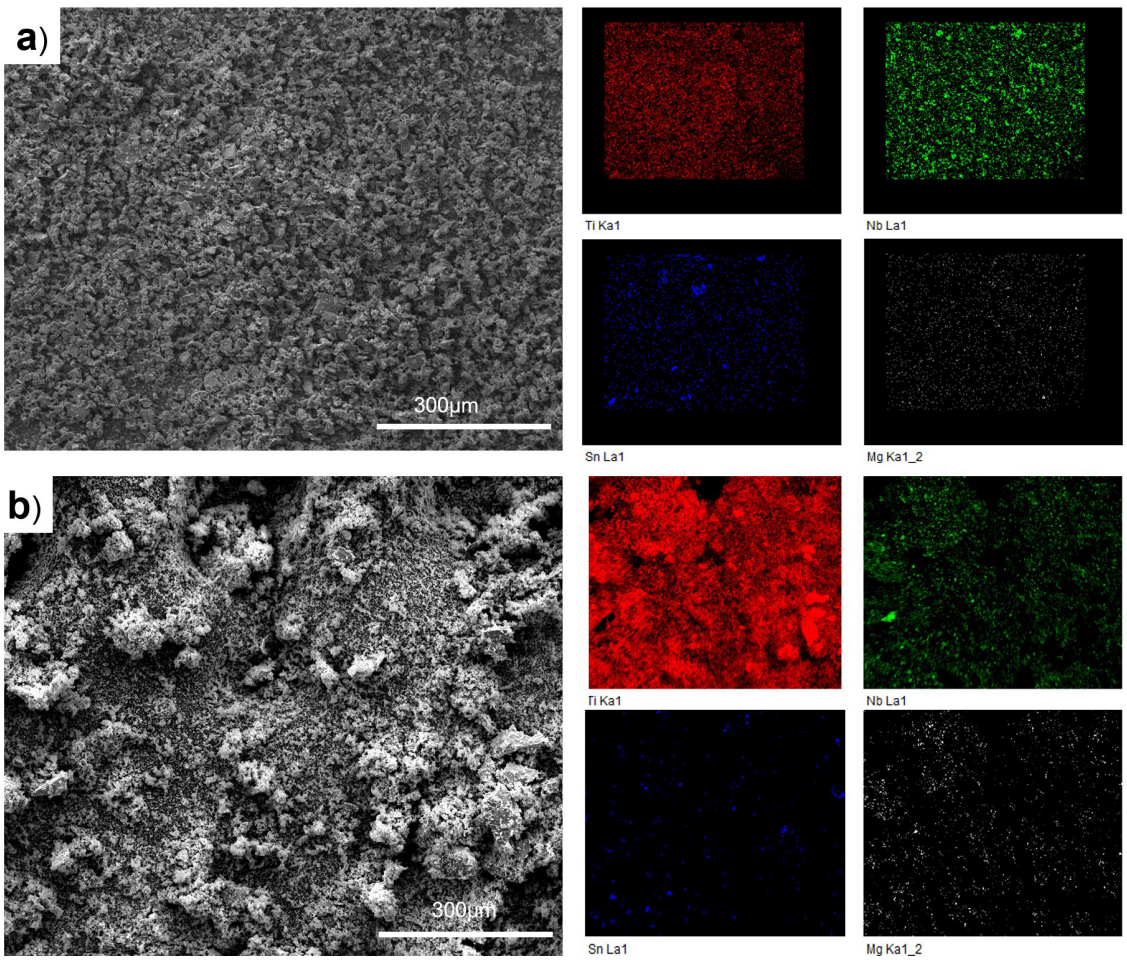


**Figure 4.** Analysis by EDS (mapping) of the elements distribution Ti, Nb, Sn and Mg in the powders after grinding at 200 rpm for a) 40 min and b) 60 min in a high energy.

Figure 5 shows the X-ray diffraction pattern of the milled samples, even without the thermal treatment with 40 min of grinding. The diffractogram is composed of diffraction patterns of all components, like Ti, Nb and Sn, with Ti under a compact hexagonal structure (hcp), (α phase), Nb under a body centered cubic structure (bcc), (β phase) and Sn under hcp phase. The mixture containing the Mg shows a peak of MgO confirming the partial oxidation of the spacer during the powder homogenization process. In addition, it is noted that the intensity of the Ti and Nb peaks in the sample with a spacer decreased. The decrease in the intensity of some Ti peaks regarding to those of Nb, mainly with Mg, may be due to the decrease of the crystal size or/and deformation of the regular arrangement and tension in the lattice during the physical actions of the high energy milling and/or change in hydride distribution of components[47].

In Table 1 is indicate the percentage content of Ti-$H_2$, Nb-$H_{0.95}$, metallic Sn and Mg after high energy milling for 40 min. In the first line are present the content of the elements without magnesium. The Nb content was increased by 10% compared to the nominal value and the metallic Sn presented a decrease of 88% compared to the nominal value. Ti-$H_2$ has a value equivalent to the nominal. The decrease in the Sn content may be related to its excellent solid solubility in the Ti lattice. Thus, at this milling stage, a part of the Sn may have been solubilized in the Ti matrix. The same is observed for the powders ground together to the However, this effect is smaller (43% reduction of Sn compared to the nominal value), as the Sn content present is significantly higher compared to milling without Mg. As Mg is much more reactive than Ti, it has a greater capacity to form oxides than Ti. As confirmed by the XRD pattern, by the presence of MgO (2θ=64.74º), the oxide layer formed reduces the effectiveness of grinding, and consequently influencing the solubility of the alloying elements in the Ti matrix. As Ti and Nb were in the form of hydrides, the oxides possibly formed were magnesium.

### *4.2. Microstructural characterization of Ti-34Nb-6Sn and Ti-34Nb-6Sn/Mg alloys by X-ray diffraction*

In the diffractograms of Figure 6, it can be seen that the temperature provided the formation of materials under two phases: α and β phase, and no Sn or Mg remained in their elementary state. There was no formation of oxides or nitrides such as TiO and TiN, as well as magnesium oxides, further no hydride peak was verified, confirming the dehydrogenation during the heat. The preliminary structural refinement showed that materials heated at 700 ºC, 44% by mass was structured under α phase and 56% under β phase, in the absence of Mg (Figure 7). In the refinement, masses of 95.734 g/unit cell (Ti) and 185.812 g/unit cell (Nb) were considered for α and β phases, respectively. In addition, it is a ternary alloy and the β phases of Ti and Nb are isomorphic with a very small difference in the lattice parameter (a = 0.33065 nm for Ti and 0.33066 nm for Nb), that is, there is no difference in the diffraction pattern. In the presence of Mg, the α phase was 43% and the β phase was 57% under the same considerations. In sintering at 800 ºC (Figure 6) without Mg, the α phase was 33% and the β phase, 67%. Regarding with Mg, the proportion was 37% and 63% α and β phases, respectively. To the both conditions, is possible affirm that not have significative difference on phases distribution.

### *4.3. SEM and EDS evaluation*

Figure 8a-d shows the micrographs obtained by a backscattered electron detector of the microstructure of the samples in different experimental conditions. The microstructure consists of regions with darker contrast, which refers to the richest Ti phases (lowest atomic number), with the

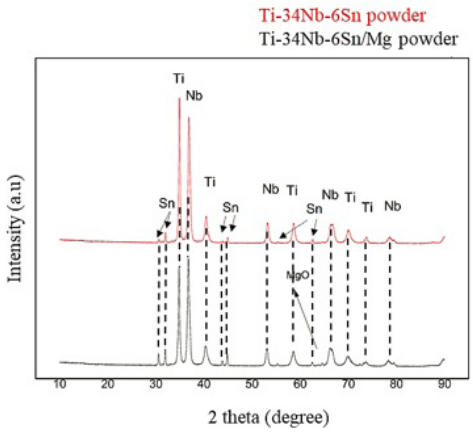


**Figure 5.** X-ray diffraction pattern of milled powders.

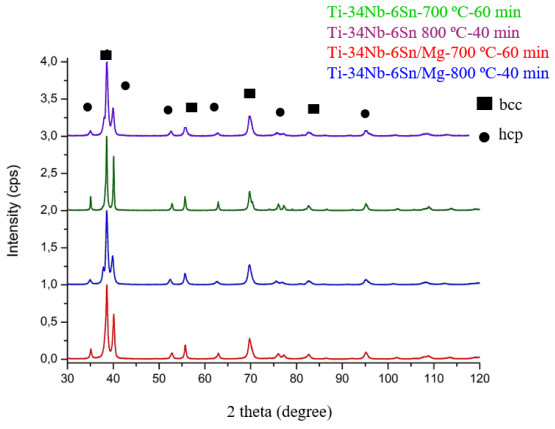


**Figure 6.** X-ray diffraction pattern of sintered samples.

**Table 1.** Rietveld refinement details for powder samples. (Ti-$H_2$: Pdf Number: 64798, Nb-$H_{0.95}$: Pdf Number: 80-2282, Tetragonal-Sn: Pdf Number: 86-2265).

| Powder Samples | Ti-$H_2$ (%) | Nb-$H_{0.95}$ (%) | Tetragonal-Sn (%) | hcp-Mg (%) |
|---|---|---|---|---|
| Ti-34Nb-6Sn | 60 | 38 | 0.71 | - |
| Ti-34Nb-6Sn/Mg | 64 | 32 | 3.4 | <1% |

hcp structure (α phase) and poor in β stabilizing elements (higher atomic radius), brighter contrast region related to the β phase richer in Nb with bcc structure and some regions with intermediate contrast, related to the β-Ti as indicated by arrows. The Nb particles in both sintering temperatures does not appear to have completely dissolved, because in the brightest contrast, the percentage of Nb is higher than Ti. In the dark contrast the percentage of Ti is higher than Nb. Note that with the increase in the sintering temperature, the regions rich in Nb decreased in size (Figure 8c, d). This decrease indicates a higher allotropic transformation due to the increase in β-*transus* temperature. The portion regarding to the brightest contrast increased with the sintering temperature, an indication there was enrichment in phases by elements of greater atomic number, not necessarily being accompanied by the formation of a homogeneous alloy. The ratio of the dark/bright area that was 41:59 without Mg changed to 43:57 (at 700 ºC) with Mg and from 26:74 to 20:80 without and with Mg, respectively, at 800 ºC (Figure 8e).

The elemental mapping of the Ti-34Nb-Sn sintered at 800 ºC is indicated in Figure 9. The Ti and Sn present better homogeneity compared to Nb particles whereas when compared to samples obtained at 700 ºC. Sn is a neutral stabilizer, its diffusion in Ti is more significant[57,58]. In addition, Sn melts first than the other materials, as it has a lower melting point (231.9 ºC). The molten Sn flows into the pores of the Ti or Nb particles by capillary forces and there its diffusion in the Ti or Nb structure is favored, being incorporate easily. In more detail, the solid solution forms when the solute atoms (like Sn) are added to the host material (Ti) then the crystal structure is maintained and no other structure is formed[28] and the solubility of Ti in liquid Sn was found to be extremely high. The solution phase formed by Sn in Ti matrix is treated as substitutional solution, and according to Wang et al.[34], the solubility of Sn in β (Ti,Nb) solid solution phase can be determined by compositions of the equilibrium phases of the typical annealed alloys, and the maximum value is 3.7-11.1 at %, which is a relative large solubility. The solubility of liquid Sn in β(Ti) is 0–11.1 at.%. The absence of Sn peaks in the XRD pattern, as well as the formation of the α and β phases may indicate their incorporation in the crystalline lattice of Ti and Nb.

### *4.4. Porosity analysis*

The total porosity found in the sintered samples is shown in Table 2. The increase in temperature did not promote a significant change in the porosity of materials without Mg. In the case of materials with Mg, the porosity increased at both temperatures compared to their respective controls. It is also noted that there was a 26% decrease in porosity with increasing temperature for materials with Mg. The porosity distribution of the samples in the different processing conditions is shown in Figure 10. Among the different temperature conditions, there are no different porosity distributions in the materials. The process involves mixing titanium powders with space-holder, compaction the mixture into green compacts, and heat treatment to burn out space-holder and sintering. The benefit of this is that it allows the extent of the porosity, the pore shape, and pore size distribution to be controlled by changing the volume fraction and shape of the space-holders. The porous materials made by the space holder technique have two types of pores: macro-pores, obtained by subsequent elimination of the space-holder material; and micro-pores, obtained by partial sintering of the titanium powder matrix.

For sintered porous materials fabricated using space-holders, the porous state cannot be defined by a single

**Table 2.** Porosity of sintered materials determined by the Archimedes method.

| Material | Total Porosity % vol (SD) |
|---|---|
| Ti-34Nb-6Sn (700 ºC) | 23±0.5 |
| Ti-34Nb-6Sn/Mg (700 ºC) | 38±0.6 |
| Ti-34Nb-6Sn (800 ºC) | 21±1.4 |
| Ti-34Nb-6Sn/Mg (800 ºC) | 28±0.3 |

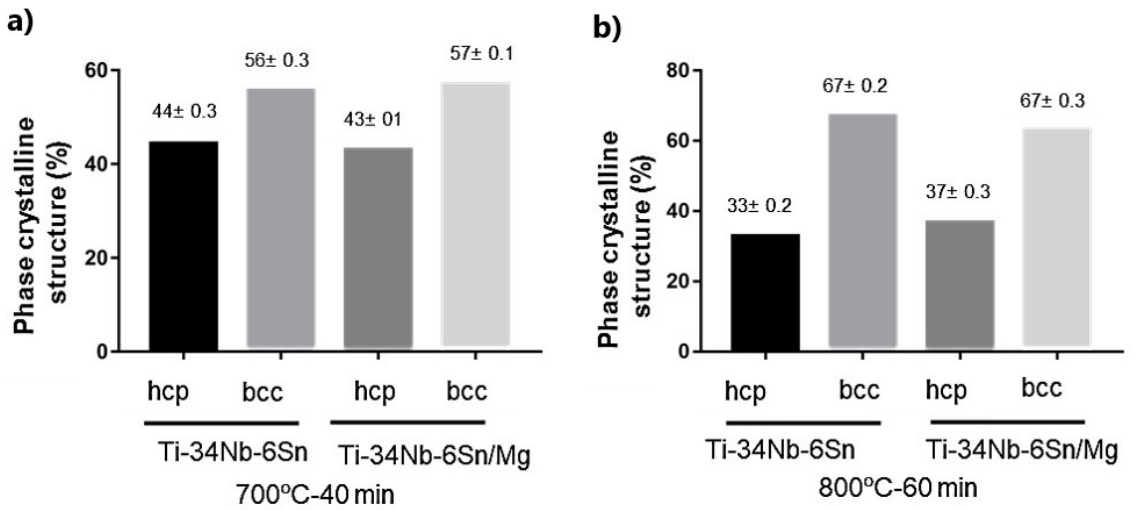


**Figure 7.** Phase crystalline structure found by X-ray diffraction and structural refinement (Rietveld method) for samples obtained by sintering at a) 700 ºC and b) 800ºC.

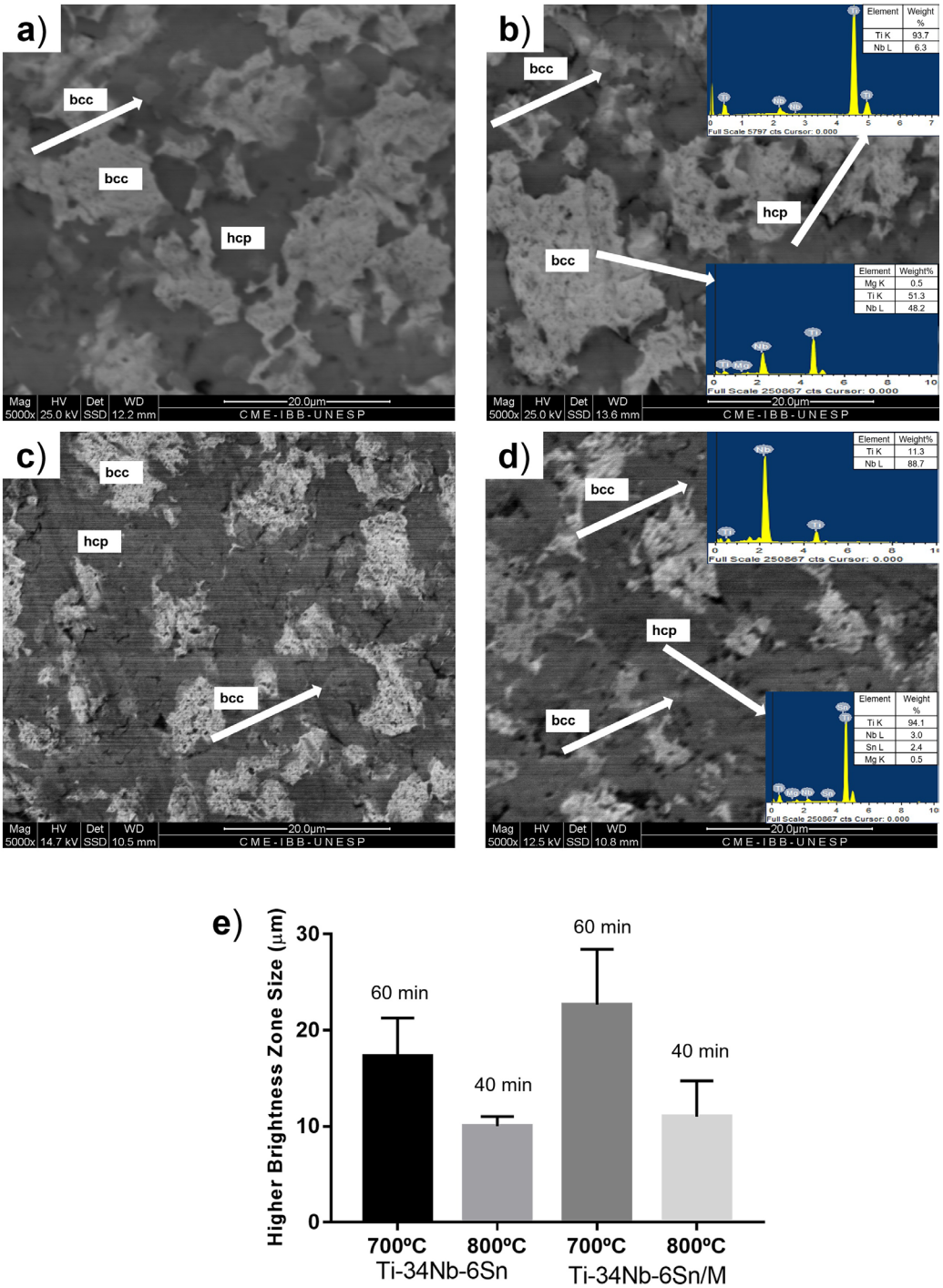


**Figure 8.** SEM of sintering materials at 700 ºC and 800 ºC. a) Ti34Nb6Sn b) Ti34Nb6Sn/Mg at 700 ºC. c) Ti34Nb6Sn D) Ti34Nb6Sn/Mg at 800 ºC. e) Quantification of the size of brightest zone on sintered materials.

parameter such as the relative density. This is because there are two inherent length scales in this material, as listed below: 1. Macro-scale pores –these are formed by the space-holder, which determines the size and morphology of these large pores. 2. Micro-scale pores –these arise due to incomplete sintering of the titanium powder. The size and morphology of these small pores are determined by the size of the constituent powder particles, and the level of compression and sintering[59].

In Figure 10a, b, both materials have macro and micropores, and with the increase in temperature there is a decrease in microporosity. With the addition of Mg, at both temperatures, the porosity increased significantly, as well as the pore size (Figure 10c, d). This increase in pore size

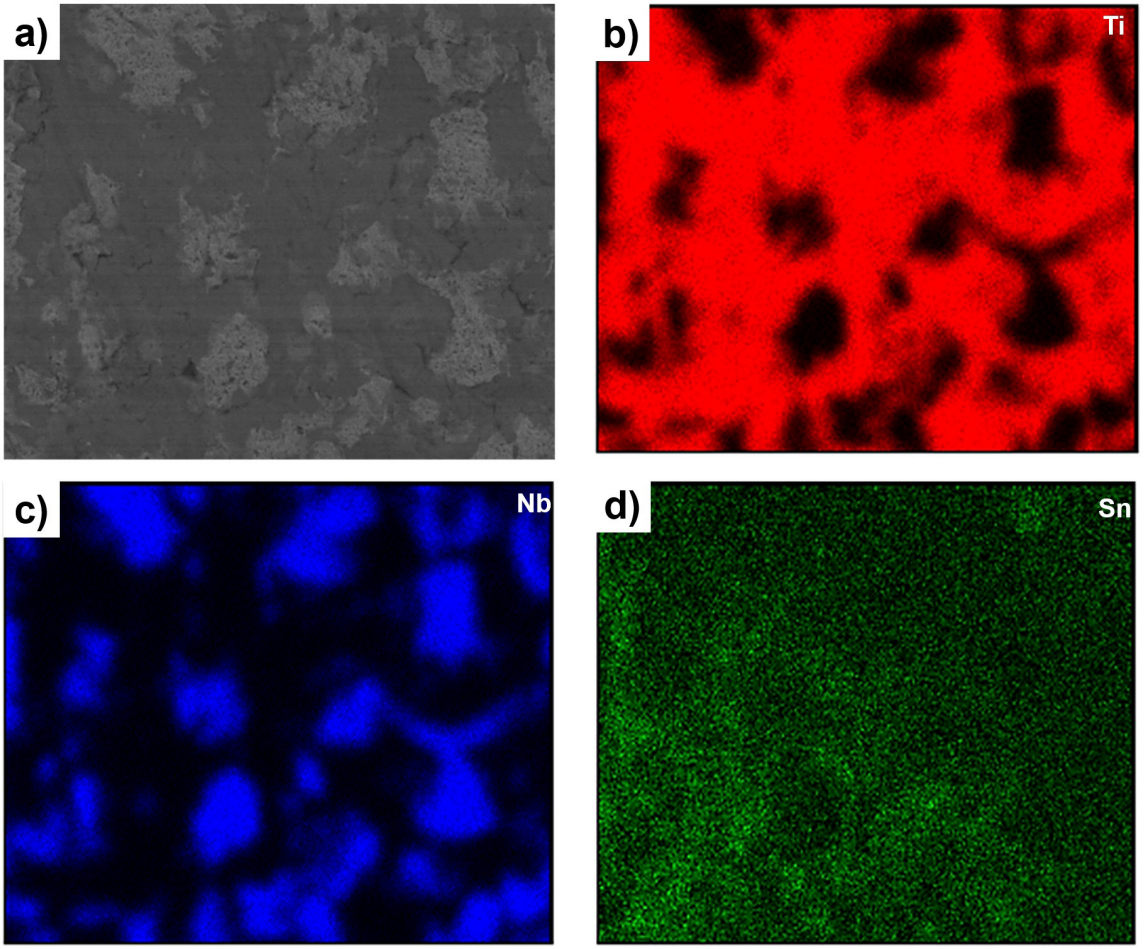


**Figure 9.** Typical element mapping by EDS of Ti-34Nb-6Sn sintered at 800 ºC. a) SEM of Ti-34Nb-6Sn sintered at 800 ºC. b), c) and d) map distribution of Ti, Nb and Sn.

is due to the size of the Mg particles that evaporated during the sintering process. It is noted that in relation to porosity, the samples are more homogeneous with the increase in the sintering temperature. This fact can be confirmed by the lower standard deviation obtained from samples sintered at 800 ºC (Figure 10e). This higher homogeneity is due to the reduction of pores of sizes smaller than 100 µm. Some studies have revealed that the optimal porosity range of an implant for bone growth is between 20 to 50%[60]. In Figure 10e, observe the pores formation increase with temperature and with the use of Mg, in the range of 98-238 µm.

This characteristic can assist in the adhesion, growth and proliferation of bone cells inside these structures[61]. The micropores have sizes in a range of 2-5 µm. According to some studies, they are classified with micropores when they are smaller than 10 µm[61]. Although some studies consider that the pores size does not influence the bone-implant interface[62], others suggest that materials with porosity in the 250-600 µm range are suitable for orthopedic application[63]. Still others have reported that pores between 100-400 µm provide sufficient permeability for bone mineralization[64]. Qualitatively, the milling of 60 min promoted higher formation of micropores compared to materials with 40 min of milling, possibly due to the smaller particle size and low sintering temperature (700 ºC)[64]. Since even increasing the porosity with the addition of Mg, at 60 min of milling, there are still micropores in the microstructure of the samples. According to some studies, micropores are not desired in the materials, as they can reduce the load-bearing cross section and consequent deterioration of the compressive strength of them[65,66]. The decrease of microporosity was also confirmed when quantifying the relative porosity of the two samples as showed in Table 2.

### *4.5. Hardness behavior*

The hardness values of the samples can be seen in Table 3. With the increase in the sintering temperature from 700 to 800 ºC the samples without magnesium increased the hardness by 4.8%. The samples with Mg increased by 30.4%. This considerable increase in hardness is due to the decrease in apparent porosity, possibly due to the higher sintering temperature and lower microporosity formed, contributing to a better homogeneity of the samples. Usually, the porosity of sintered materials decreases, and the distribution of pores changes with increasing temperature, since the mass transport

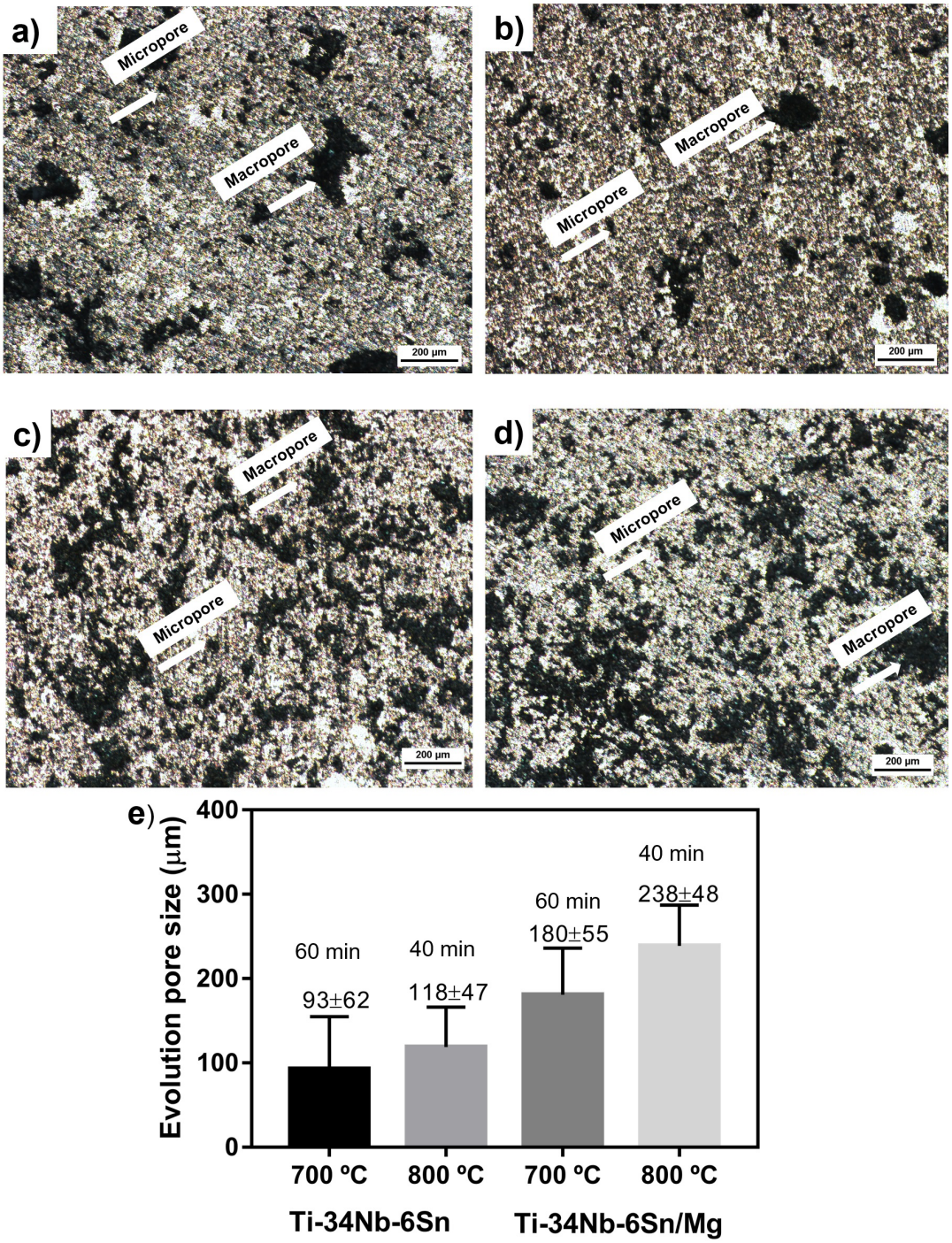


**Figure 10.** Micrograph of the pore distribution of sintered materials under different experimental conditions. a) and b) referring to samples Ti-34Nb-6Sn at 700 ºC and 800 ºC. c) and d) referring to Ti-34Nb-6Sn / Mg samples sintered at 700 ºC and 800 ºC. e). Evolution of pore size evaluation on the samples by Image J software.

**Table 3.** Vickers hardness analysis.

| Material | Temperature | Hardness (HV) |
|---|---|---|
| Ti-34Nb-6Sn | 700 ºC | 146±16 |
| Ti-34Nb-6Sn/Mg | 700 ºC | 92±10 |
| Ti-34Nb-6Sn | 800 ºC | 153±12 |
| Ti-34Nb-6Sn/Mg | 800 ºC | 120±20 |

is greater at higher temperatures, which leads to greater formation of more efficient particle-to-particle bonds[67]. In the case of samples without Mg, the porosity (Table 2), did not change significantly. It is evident that the mass transport occurred as changes in the fraction of phase and porosity distribution were observed. The temperature effect

was higher for samples containing Mg, probably because its evaporation is more intense in the temperature range used. The Mg effect was less for the synthesis at 800 ºC, with smaller difference either between the hardness, as well as the effect of temperature on the hardness, porosity and fraction of β phase was higher in the samples with Mg. It should be remembered that the composition of Mg determined by EDS is not accurate due to the low content of this element in the samples. The hardness values found are significantly close to the Ti-CP (136 HV), considering that the fraction of α and β phases and microstructures are different from those of the present work[68]. In similar alloys, the hardness value found was 158 HV for Ti-33.6Nb4Sn[69] and 173 HV for Ti-30Nb-4Sn[70]. Since the hardness and porosity ratio of materials applied to orthopedics is extremely important to mimic the bone tissue, the hardness of the materials synthesized here is similar to materials already commercialized[71].

### *4.6. Biological effect caused by the treatment of BMMSCs after 24 hours in contact with alloys*

Figure 11 represents the biological effect of the conditioned medium with the materials obtained by sintering at 800 ºC, that present better homogeneity in they microstructure. Note that there was no significant difference (P> 0.05) in cell viability after 24 h of culture using conditioned medium with samples compared with the control group. This finding may be due to the absence of ions or toxic particles released in the culture medium, not influencing the viability of the cells. This analysis is extremely important, because in a biological environment, the first contact with the biomaterial is made by stem cells that will later differentiate into bone cells and adhere to the implant, allowing for good osteointegration[72].

### *4.7. BMMSCS adhesion on the alloys surface*

In the 72-h growth test, the cells adhered to practically the entire surface of the material, as well as inside the pores (Figure 12a-d). It is not possible to quantify the adhered cells, however, cell proliferation and adhesion were very good in all materials. It is also noted that after 72 h in direct contact with the surface of the materials, the morphology of the cells is more circular in the materials with Mg (Figure 12c and 12d compared to materials without Mg (Figure 12a and 12b). This may be due to two factors: greater porosity formation and the preference of the cells for these rougher regions, which mimic the natural bone tissue. However, at 700 ºC the cell filopodia are observed, which would indicate the best adhesion, while at 800 ºC the cells are more rounded and, in all cases, present formation of adhesion filopodia. A second factor to be taken into account would be Mg, which has not completely evaporated. It can assist in the adhesion of cells, as it increases the osteoconductivity of the material (property of indicating the path for bone growth, on the surface or pores). Divalent ions such as $Mg^{2+}$, $Ca^{2+}$ or $Mn^{2+}$ can bind to sites present in the extracellular domain of the integrin subunits[73], which are transmembrane proteins responsible for cell adhesion[74].

## 5. Conclusions

- Hydride and dehydride process of titanium and niobium powders was confirmed by the XRD patterns, as well as the formation of brittle particles in order to optimize the milling process;
- All samples were structured under α and β phase, and samples that received Mg as a spacer had slightly lower β phase content compared to samples without Mg, suggesting that greater porosity formation may influence the α→β transformation process due to the presence of barriers formed by pores;
- Mg provided greater porosity formation, and at 800ºC the formation of micropores decreased, due to better sintering of the materials;
- Materials milled in a shorter time promoted a significant increase in the formation of macropores;
- Hardness obtained for materials without Mg at 700 and 800ºC and for materials with Mg obtained at 800ºC presented values close to commercialized materials and also to others with similar nominal composition;
- Cells treated with conditioned medium with the samples that received Mg showed cell viability

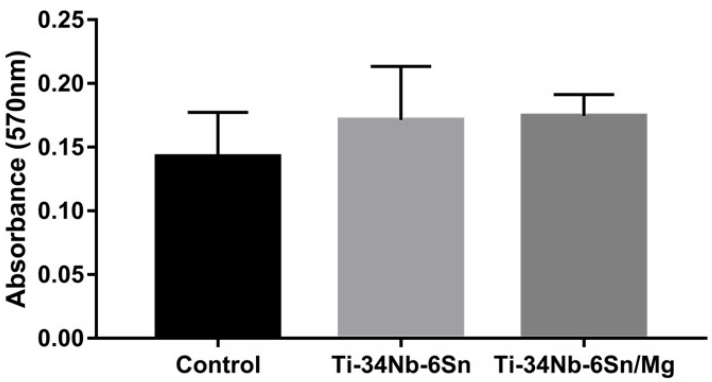


**Figure 11.** Cell viability of BMMSCs after 24 h of culture in a conditioned medium with the samples sintered at 800 ºC. Absorbance measurements performed using a 570 nm microplate reader.

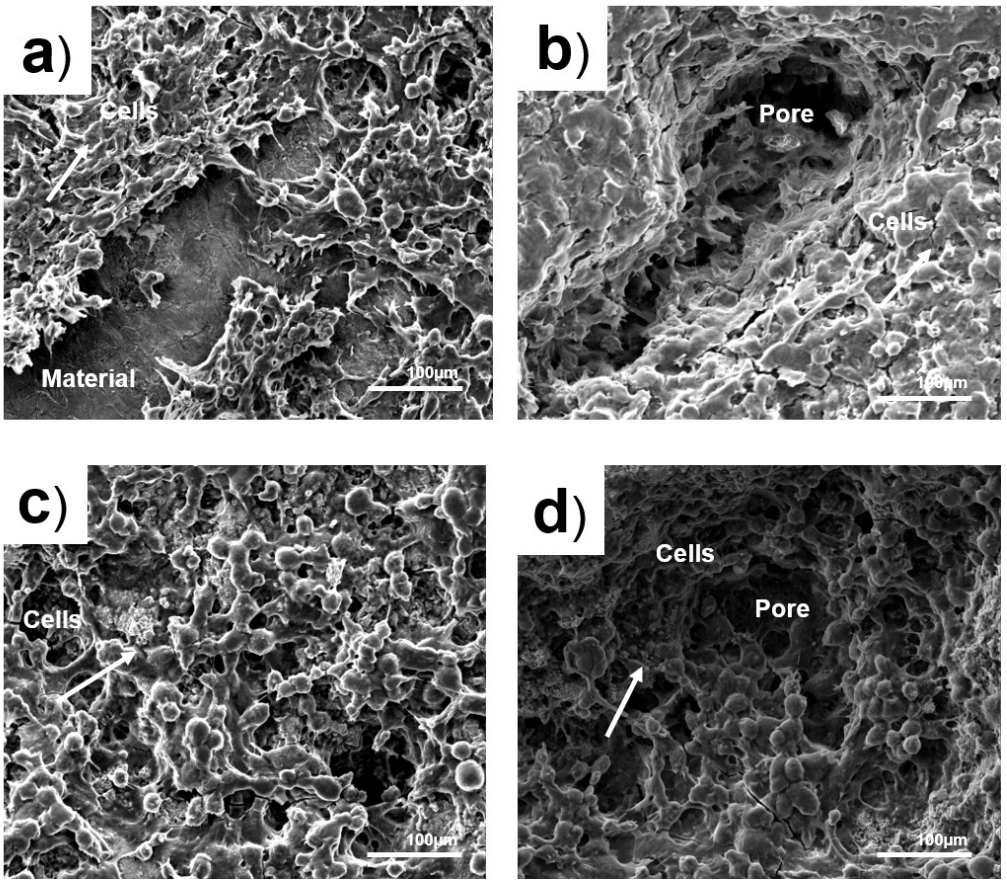


**Figure 12.** SEM of the BMMSCs adhered on the samples after 48 h culture a) sample sintered at 700 ºC without Mg; b) sample sintered at 800 ºC without Mg; c) sample sintered at 800 ºC with Mg and d) sample sintered at 800 ºC with Mg.

comparable to the control group, and after 48 h of cell culture on the samples, there was significant growth; cells that grew under the Mg-containing materials showed more circular morphology, an indication of possible cell differentiation;

## 6. Acknowledgments

This work was supported by Fundação de Amparo à Pesquisa do Estado de São Paulo (FAPESP) [grant: 2017/13876-2; 2019/ 24237-6] and CAPES, for scholarships, and the Instituto de Pesquisas Tecnológicas do Estado de São Paulo, in the development of materials, whom the authors thank.

## 7. References

1. Lewallen EA, Riester SM, Bonin CA, Kremers HM, Dudakovic A, Kakar S, et al. Biological strategies for improved osseointegration and osteoinduction of porous metal orthopedic implants. Tissue Eng Part B Rev. 2015;21(2):218-30. http://dx.doi.org/10.1089/ten.teb.2014.0333.
2. Geetha M, Singh AK, Asokamani R, Gogia AK. Ti based biomaterials, the ultimate choice for orthopaedic implants: a review. Prog Mater Sci. 2009;54(3):397-425. http://dx.doi.org/10.1016/j.pmatsci.2008.06.004.
3. Kulkarni M, Mazare A, Schmuki P, Iglic A. Biomaterial surface modification of titanium and titanium alloys for medical applications. In: Seifalian A, Mel A, Kalaskar DM, editors. Nanomedicine. Manchester: One Central Press; 2014. p. 111-33.
4. Davis JR. Handbook of materials for medical devices. 4th ed. Novelty: ASM International; 2006.
5. Niinomi M, Narushima T, Nakai M. Advances in metallic biomaterials. Berlin: Springer; 2015.
6. Churakova D, Gunderov D, Lukyanov A, Nollmann N. Transformation of the TiNi alloy microstructure and the mechanical properties caused by repeated B2-B190 martensitic transformations. Chin Shu Hsueh Pao. 2015;28(10):1230-7.
7. Lin YC, Chen HM, Chen YC. The effect of different methods to add nitrogen to titanium alloys on the properties of titanium nitride clad layers. Mater Des. 2014;54:222-9. http://dx.doi.org/10.1016/j.matdes.2013.08.069.
8. Feng GJ, Li ZR, Liu RH, Feng SC. Effects of joining conditions on microstructure and mechanical properties of Cf/Al composites and TiAl alloy combustion synthesis joints. Chin Shu Hsueh Pao. 2015;28:405.
9. Vasconcellos LMR, Rodarte Y, do Prado RF, de Vasconcellos LGO, Alencastro Gra MLD, Alves CA. Porous titanium by powder metallurgy for biomedical application: characterization, cell citotoxity and in vivo tests of osseointegration. In: Reditor H, editor. Biomedical engineering: technical applications in medicine. London: IntechOpen; 2012. http://dx.doi.org/10.5772/47816.
10. Cremasco A, Messias AD, Esposito AR, Duek EAR, Caram R. Effects of alloying elements on the cytotoxic response of titanium alloys. Mater Sci Eng C. 2011;31(5):833-9. http://dx.doi.org/10.1016/j.msec.2010.12.013.

11. Barceloux DG, Barceloux D. Vanadium. J Toxicol Clin Toxicol. 1999;37(2):265-78. http://dx.doi.org/10.1081/CLT-100102425.
12. Marquis JK. Aluminum neurotoxicity: an experimental perspective. Bull Environ Contam Toxicol. 1982;29(1):43-9. http://dx.doi.org/10.1007/BF01606087. PMid:6981444.
13. Miura K, Yamada N, Hanada S, Jung T-K, Itoi E. The bone tissue compatibility of a new Ti–Nb–Sn alloy with a low Young's modulus. Acta Biomater. 2011;7(5):2320-6. http://dx.doi.org/10.1016/j.actbio.2011.02.008. PMid:21316491.
14. Matsumoto H, Watanabe S, Hanada S. Beta TiNbSn alloys with low Young's modulus and high strength. Mater Trans. 2005;46(5):1070-8. http://dx.doi.org/10.2320/matertrans.46.1070.
15. Vasconcellos LMR, Cairo CAA, Vasconcellos LGO, Alencastro Graça ML, Prado RF, Carvalho YR. Porous titanium by powder metallurgy for biomedical application: characterization, cell citotoxity and in vivo tests of osseointegration. In: Hudak R, Penhaker M, Majernik J, editors. Biomedical engineering: technical applications in medicine. London: IntechOpen; 2012.
16. Tal-Gutelmacher E, Eliezer D. The hydrogen embrittlement of titanium-based alloys. J Manage. 2005;57:46-9. http://dx.doi.org/10.1007/s11837-005-0115-0.
17. Kennedy AR, Lopez VH. The decomposition behavior of as-received and oxidized TiH2 foaming-agent powder. Mater Sci Eng A. 2003;357(1-2):258-63. http://dx.doi.org/10.1016/S0921-5093(03)00211-9.
18. Ma M, Liang L, Wang L, Wang Y, Cheng Y, Tang B, et al. Phase transformations of titanium hydride in thermal desorption process with different heating rates. Int J Hydrogen Energy. 2015;40(29):8926-34. http://dx.doi.org/10.1016/j.ijhydene.2015.05.083.
19. Tao SC, Xu JL, Yuan L, Luo JM, Zheng YF. Microstructure, mechanical properties and antibacterial properties of the microwave sintered porous Ti–3Cu alloys. J Alloys Compd. 2020;812:152142. http://dx.doi.org/10.1016/j.jallcom.2019.152142.
20. Lai T, Xu J-L, Xiao Q-F, Tong Y-X, Huang J, Zhang J-P, et al. Preparation and characterization of porous NiTi alloys synthesized by microwave sintering using Mg space holder. Trans Nonferrous Met Soc China. 2021;31(2):485-98. http://dx.doi.org/10.1016/S1003-6326(21)65511-5.
21. Liang G, Schulz R. Synthesis of Mg-Ti alloy by mechanical alloying. J Mater Sci. 2003;38(6):1179-84. http://dx.doi.org/10.1023/A:1022889100360.
22. Murray JL. The Mg-Ti (magnesium-titanium) system. Bull Alloy Phase Diagr. 1986;7(3):245-8. http://dx.doi.org/10.1007/BF02868999.
23. Mansourighasri A, Muhamad N, Sulong A. Processing titanium foams using tapioca starchas a space holder. J Mater Process Technol. 2012;212(1):83-9. http://dx.doi.org/10.1016/j.jmatprotec.2011.08.008.
24. Nakas GI, Dericioglu AF, Bor S. Monotonic and cyclic compressive behavior of superelastic TiNi foams processed by sintering using magnesium space holder technique. Mater Sci Eng A. 2013;582:140-6. http://dx.doi.org/10.1016/j.msea.2013.06.011.
25. Nayeb-Hashemi AA, Clark JB. Phase diagrams of binary magnesium alloys. Metals Park: ASM International; 1988.
26. Benjamin JS. Dispersion strengthened superalloys by mechanical alloying. Metall Mater Trans, A Phys Metall Mater Sci. 1970;1:294351.
27. Rajeshkanna S, Nirmalkumar O. Synthesis and characterization of Cu nanoparticle using high energy ball milling route and compare with Scherrer Equation. Int J Sci Eng. 2014;2:305.
28. Murray JL. The Sn-Ti (Tin-Titanium) system. In: Murray JL, editor. Phase diagrams of binary titanium alloys. Materials Park: ASM International; 1987. 294 p. (vol. 1).
29. Liu C, Klotz U, Uggowitzer P, Löffler JF. Thermodynamic assessment of the Sn-Ti system. Monatsh Chem. 2005;136(11):1921-30. http://dx.doi.org/10.1007/s00706-005-0392-x.
30. Antipov AI, Moiseev VN. Coefficient of β-stabilization of titanium alloys. Metal Sci Heat Treat. 1997;39(12):499-503. http://dx.doi.org/10.1007/BF02471366.
31. Moiseev VN, Sholokhova LV, Terent'eva LN. Self-hardening titanium alloy. Tekhnol Lyogkikh Splavov. 1976;5:13-20.
32. Toffolon C, Servant C, Sundman B. Thermodynamic assessment of the Nb-Sn system. J Phase Equilibria. 1998;19(5):479-85. http://dx.doi.org/10.1361/105497198770341978.
33. Zhang YL, Liu HS, Jin ZP. Thermodynamic Assessment of the Nb-Ti System. Calphad. 2001;25(2):305-17. http://dx.doi.org/10.1016/S0364-5916(01)00051-7.
34. Wang JL, Liu LB, Zhang XD, Bai WM, Chen CP. Isothermal section of the Ti-Nb-Sn ternary system at 700 ºC. J Phase Equilibria. 2014;35(3):223-31. http://dx.doi.org/10.1007/s11669-014-0295-9.
35. Rossi MC, Bayerlein DL, Brandão JS, Pfeifer JPH, Rosa GS, Silva WM, et al. Physical and biological characterizations of TiNbSn/(Mg) system produced by powder metallurgy for use as prostheses material. J Mech Behav Biomed Mater. 2021;115:104260. http://dx.doi.org/10.1016/j.jmbbm.2020.104260. PMid:33484993.
36. Rossi MC, Bayerlein DL, Gouvêa ES, Haro Rodríguez MV, Escuder AV, Borrás VA. Evaluation of the influence of low Mg content on the mechanical and microstructural properties of beta titanium alloy. Journal of Materials Research and Technology. 2021;10:916-25. http://dx.doi.org/10.1016/j.jmrt.2020.12.103.
37. Larson AC, Von Dreele RB. General Structure Analysis System (GSAS). New Mexico: Los Alamos National Laboratory; 2000. p. 86-748. (Report LAUR).
38. ASTM: American Society for Testing and Materials. ASTM E92-82: standard test method for vickers hardness of metallic materials. West Conshohocken: ASTM International; 2003.
39. Viana ACD, Gonzalez BM, Buono VTL, Bahia MGA. Influence of sterilization on mechanical properties and fatigue resistance of nickel–titanium rotary endodontic instruments. Int Endod J. 2006;39(9):709-15. http://dx.doi.org/10.1111/j.1365-2591.2006.01138.x.
40. Neuss S, Panfil C, Duarte Campos DF, Weber M, Otten C, Reisgen U, et al. Adhesion of human mesenchymal stem cells can be controlled by electron beam-microstructured titanium alloy surfaces during osteogenic differentiation. Biomed Eng. 2015;60:215-23.
41. Duvvuru MK, Han W, Chowdhury PR, Vahabzadeh S, Sciammarella F, Elsawa SF. Bone marrow stromal cells interaction with titanium: effects of composition and surface modification. PLoS One. 2019;14(5):e0216087. http://dx.doi.org/10.1371/journal.pone.0216087. PMid:31116747.
42. Jarolimova P, Voltrova B, Blahnova V, Sovkova V, Pruchova E, Hybasek V, et al. Mesenchymal stem cell interaction with Ti6Al4V alloy pre-exposed to simulated body fluid. RSC Advances. 2020;10(12):6858-72. http://dx.doi.org/10.1039/C9RA08912H.
43. Wang Y, Yu Z, Guo X, Hu J. Surface morphology of modified titanium alloy affects proliferation stability of bone marrow mesenchymal stem cells. Surf Coat Tech. 2019;366:156-63. http://dx.doi.org/10.1016/j.surfcoat.2019.02.087.
44. Huo S-C, Yue B. Approaches to promoting bone marrow mesenchymal stem cell osteogenesis on orthopedic implant surface. World J Stem Cells. 2020;12(7):545-61. http://dx.doi.org/10.4252/wjsc.v12.i7.545. PMid:32843913.
45. Haleem-Smith H, Argintar E, Bush C, Hampton D, Postma WF, Chen FH, et al. Biological responses of human mesenchymal stem cells to titanium wear debris particles. J Orthop Res. 2012;30(6):853-63. http://dx.doi.org/10.1002/jor.22002. PMid:22083964.
46. Suryanarayana C. Mechanical alloying and milling. Prog Mater Sci. 2001;46(1-2):1-184. http://dx.doi.org/10.1016/S0079-6425(99)00010-9.

47. Nouri A, Hodgson PD, Wen C. Effect of ball-milling time on the structural characteristics of biomedical porous Ti–Sn–Nb alloy. Mater Sci Eng C. 2011;31(5):921-8. http://dx.doi.org/10.1016/j.msec.2011.02.011.
48. Kulov A, Gusev A. Phase equilibria in the W-C system and tungsten carbides. Russ Chem Rev. 2006;75:687-708. http://dx.doi.org/10.1070/RC2006v075n07ABEH003606.
49. Al-Qureshi HA, Galiotto A, Klein AN. On the mechanical of cold die compaction for powder metallurgy. J Mater Process Technol. 2005;166(1):135-43. http://dx.doi.org/10.1016/j.jmatprotec.2004.08.009.
50. Dercz G, Matuła I, Zubko M, Dercz J. Phase composition and microstructure of new Ti–Ta–Nb–Zr biomedical alloys prepared by mechanical alloying method. Powder Diffr. 2017;32(S1):S186. http://dx.doi.org/10.1017/S0885715617000045.
51. Hewitt SA, Laoui TE, Kibble KK. Effect of milling temperature on the synthesis and consolidation of nanocomposite WC–10Co powders. Int J Refract Met Hard Mater. 2009;27(1):66-73. http://dx.doi.org/10.1016/j.ijrmhm.2008.03.007.
52. Heckel RW. Density-pressure relationships in powder compaction. Trans Metall Soc AIME. 1961;221:671-5.
53. Wert JE, Paton NE. Enhanced superplasticity and strength in modified Ti-6AI-4V alloys. Metall Mater Trans, A Phys Metall Mater Sci. 1983;14(12):2535-44. http://dx.doi.org/10.1007/BF02668895.
54. Hida M, Asai K, Takemoto Y, Sakakibara A. Solid solubility in nanocrystalline Ti/Mg and Mg/Ti composites powder produced by mechanical alloying. Mater Sci Forum. 1997;235:187-92.
55. Hewitt SA, Laoui TE, Kibble KK. Effect of milling temperature on the synthesis and consolidation of nanocomposite WC-10Co powders. Int J Refract Met Hard Mater. 2009;27(1):66-73. http://dx.doi.org/10.1016/j.ijrmhm.2008.03.007.
56. Bokshtein SZ, Kishkin ST, Osvenskii VB. The effect of polymorphic transformation on diffusion in titanium. Metal Sci Heat Treat. 1960;2(6):329-32. http://dx.doi.org/10.1007/BF00715783.
57. Biesiekierski A, Wang J, Gepreel MA, Wen C. A new look at biomedical Ti-based shape memory alloys. Acta Biomater. 2012;8(5):1661-9. http://dx.doi.org/10.1016/j.actbio.2012.01.018. PMid:22326786.
58. Li Y, Yang C, Zhao H, Qu S, Li X, Li Y. New developments of ti-based alloys for biomedical applications. Materials. 2014;7(3):1709-800.
59. Niu W, Gill S, Dong H, Bai C. A new two-scale model for predicting elastic properties of porous titanium formed with space-holders. Comput Mater Sci. 2010;50(1):172-8. http://dx.doi.org/10.1016/j.commatsci.2010.07.022.
60. Cook SD, Walsh KA, Haddad RJ Jr. Interface mechanics and bone growth into porous Co–Cr–Mo alloy implants. Clin Orthop Relat Res. 1985;193(&NA;):271-80. http://dx.doi.org/10.1097/00003086-198503000-00037. PMid:3971631.
61. Nouri A, Hodgson PD, Wen C. Biomimetic porous titanium scaffolds for orthopedic and dental applications. In: Mukherjee A, editor. Biomimetics learning from nature. London: IntechOpen; 2010. p. 415-50.
62. Mishra S, Knothe-Tate ML. Effect of lacunocanalicular architecture on hydraulic conductance in bone tissue: implications for bone health and evolution. Anat Rec A Discov Mol Cell Evol Biol. 2003;273A(2):752-62. http://dx.doi.org/10.1002/ar.a.10079. PMid:12845711.
63. Dabrowski B, Swieszkowski W, Godlinski D, Kurzydlowski J. Highly porous titanium scaffolds for orthopaedic applications. J Biomed Mater Res B Appl Biomater. 2010;95B(1):53-61. http://dx.doi.org/10.1002/jbm.b.31682. PMid:20690174.
64. Arifvianto B, Zhou J. Fabrication of metallic biomedical scaffold with the space holder method: a review. Mater. 2014;7(5):3588-622. http://dx.doi.org/10.3390/ma7053588. PMid:28788638.
65. Kotan G, Bor AS. Production and characterization of high porosity Ti-6Al-4V foam by space holder technique powder metallurgy. Turkish J Eng Environ Sci. 2007;31:149-56.
66. Niu W, Bai C, Qiu G, Wang Q. Processing and properties of porous titanium using space holder technique. Mater Sci Eng A. 2009;506(1-2):148-51. http://dx.doi.org/10.1016/j.msea.2008.11.022.
67. German RM. Powder metallurgy science. New York: Metal Powder Industry Federation; 1990.
68. Fleischer RL, Gilmore RS, Zabala RJ. Elastic moduli of polycrystalline, intermetallic compounds of titanium. J Appl Phys. 1988;64(6):2964-7. http://dx.doi.org/10.1063/1.341558.
69. Ozaki T, Matsumoto H, Watanabe S, Hanada S. Beta Ti alloys with low Young's Modulus. Metall Mater Trans. 2004;45(8):2776-9. http://dx.doi.org/10.2320/matertrans.45.2776.
70. Salvador CAF, Lopes ESN, Ospina CA, Caram R. Orthorhombic martensite formation upon aging in a Ti-30Nb-4Sn alloy. Mater Chem Phys. 2016;183:238-46. http://dx.doi.org/10.1016/j.matchemphys.2016.08.023.
71. Bandyopadhyay A, Espana F, Balla VK, Bose S, Ohgami Y, Davies NM. Influence of porosity on mechanical properties and in vivo response of Ti6Al4V implants. Acta Biomater. 2010;6(4):1640-8. http://dx.doi.org/10.1016/j.actbio.2009.11.011. PMid:19913643.
72. Bruder SP, Jaiswal N, Ricalton NS, Mosca JD, Kraus KH, Kadiyala S. Mesenchymal stem cells in osteobiology and applied bone regeneration. Clin Orthop Relat Res. 1998;355S(355, Suppl.):S247-56. http://dx.doi.org/10.1097/00003086-199810001-00025. PMid:9917644.
73. Zreiqat H, Howlett C, Zannettino A, Evans P, Schulze-Tanzil G, Knabe C, et al. Mechanisms of magnesium-stimulated adhesion of osteoblastic cells to commonly used orthopaedic implants. J Biomed Mater Res. 2002;62(2):175-84. http://dx.doi.org/10.1002/jbm.10270. PMid:12209937.
74. Anselme K. Osteoblast adhesion on biomaterials. Biomaterials. 2000;21(7):667-81. http://dx.doi.org/10.1016/S0142-9612(99)00242-2. PMid:10711964.